

# Experimental investigation and validation of structural properties of a new design for active twist rotor blades

Steffen Kalow\* - Steffen.Kalow@dlr.de; Bram van de Kamp\* - Bram.vandeKamp@dlr.de;  
Ralf Keimer\* - Ralf.Keimer@dlr.de; Johannes Riemenschneider\* - Johannes.Riemenschneider@dlr.de

\*Institute for Composite Structures and Adaptive Systems  
German Aerospace Center - DLR  
Braunschweig, Germany

## Abstract

Vibration and noise are omnipresent in a helicopter environment and therefore their reduction is an important goal in helicopter research. Actuators embedded into the skin of a helicopter rotor blade can produce a twist, which influences the propagation of the air turbulence. Hence, vibration and noise levels can be significantly reduced. An important issue during operation of a rotor blade are the centrifugal loads which affect the actuators and can cause failure. Based on the German Aerospace Center (DLR) project STAR, the design of an active twist rotor blade has been adapted, such that the loads in the actuator system can be significantly reduced and furthermore distributed evenly. Besides a new actuator design, described in an earlier study of the authors, this paper focus on the use of carbon fiber composite for the spar and additional straps near to the trailing edge. This increases the durability of a new generation of active twist rotor blades, which is the basis for a specific and efficient use of the active twist technology. A first prototype of the new designed rotor blade has already been built. The design changes are addressed in this paper as well as parts of the manufacturing process. Also results of the numerical model are validated experimentally and blade properties of the prototype blade are presented.

## 1 INTRODUCTION

The basic principle of individual blade control and its benefits for an improved aerodynamic behavior has been shown in many different studies<sup>[2]</sup>. The goals of helicopter research are vibration and noise reduction as well as performance improvement. Active twist rotors can actively contribute to this. Embedded in the skin of a rotor blade, piezo-ceramic actuators are able to twist the entire rotor blade and thus influence the propagation of air vortices. For several years the German Aerospace Center investigates this technology and built several model rotor blades. A history of these activities can be found in<sup>[3;4;5]</sup>. In 2009 the German Aerospace Center started its efforts in designing and manufacturing a Smart Twisting Active Rotor (STAR) in a consortium with international partners, being the US Army Aeroflightdynamics Directorate (AFDD), NASA, ONERA, JAXA, Konkuk University and KARI. A wind tunnel test in the large low-speed facility of the German-Dutch Wind Tunnel (DNW), with these rotor blades was scheduled in 2013. Within the pre-testing of the STAR rotor at DLR the functionality of active twist blades and the rotor test stand could be demonstrated successfully, but then fatigue problems occurred during subsequent tests. Extensive investigations were conducted to find out the causes of failure. The results of these investigations were presented for the

first time at the AHS 2016 in West Palm Beach (Florida, US)<sup>[6]</sup>. Rotor blades are exposed to enormous loads resulting mainly from the centrifugal forces, which are the main reason for the actuator failures. Based on these findings the actuator and the rotor blade design were completely revised.



Figure 1: STAR rotor with previous design

Objective of the prototype blade design is a robust structure leading to a longer durability of the actuators. Cracks in the ceramics of the actuators were to be avoided or at least reduced to a minimum. In order to achieve this, the

structure has to reduce the occurring loads and provide an even strain distribution within the actuators in order to prevent damages. This paper is based on AHS publication<sup>[6]</sup>. Only the main design changes are reviewed here. The finite element (FE) model is validated by the experimentally determined blade properties of the prototype blade. These results, including static twist, bending, torsional stiffness and axis positions are also presented in the paper, as well as insights into the manufacturing process of the prototype blade.

## 2 BLADE DESIGN - CHANGES AND THEIR EFFECTS

The main objective of the new design is to reduce the overall actuator strain, which results from the static and dynamic loads. In previous designs the actuators strains were very high especially at the trailing edge. Simultaneously, all other constraints, concerning for example active twist, strength analysis and dynamic properties, still have to be considered and satisfied. Many properties depend on each other, thus an iterative approach is necessary to find a design meeting all given constraints. Figure 2 shows the calculated strain distribution under pure centrifugal loads over the chord length for both designs. The orange curve represents the reference blade with an old design from 2011 and shows very clearly that the strains at the trailing edge are much higher than the strains at the leading edge. The reason for this unequal distribution of loads was found in the position of the tension axis. If the tension and the center of gravity axis of the blade are not exactly at the same position, the blade deforms sickle-shaped under centrifugal loads.

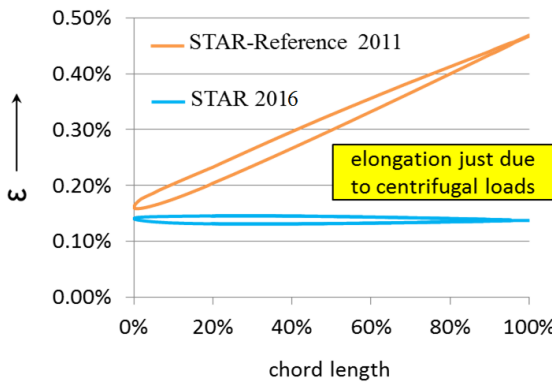


Figure 2: Chordwise strain distribution near the blade root

In this case, this means that the position of the tension axis was clearly ahead the position of the center of gravity, which is at about a quarter of the chord length. Therefore the rotor blade pivoted towards the leading edge. This lag bending led to very high loads in the actuators at the trailing edge, especially in the root area. In<sup>[6]</sup> the failure mechanisms were shown and a allowable strain level for the ac-

tuators was identified. The simulation results are shown by the blue curve in figure 2.

Since the rotor blade shape originates from the BO105, its aerodynamic profile does not change over the radius. An active twist blade cross section including skin, actuators, spar, nose balance weight and cables for instrumentation is shown in figure 3. The upper cross section shows the former design from 2011, the lower cross section shows the new design from 2016. The aerodynamic shape of the blades was not changed.

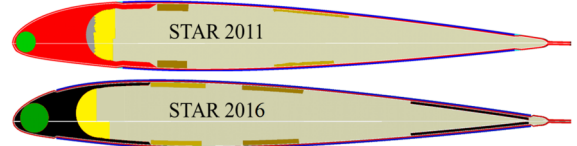


Figure 3: Comparison of old and new rotorblade design

The inner design on the other hand underwent some major changes which are presented here:

- A CFRP spar (black) with a reduced cross section by 35% and an increased tensile stiffness replaced the former GFRP spar (red)
- CFRP straps (black) near the trailing edge move the tension center in the direction of the trailing edge. The dimensioning of the straps provides a uniform elongation for the whole cross section under pure tension respectively the centrifugal loads
- The combination of both components reduces the strains under centrifugal force at the trailing by about 70% and the resulting elongation does not exceed 0.18% .
- Increasing the tensile stiffness also affects the lead lag and flap bending stiffness and increases it significantly
- Torsional stiffness remains nearly the same
- Due to the high instrumentation and the CFRP straps, the balancing weight had to be enlarged by a factor of 1.5, causing a 10% mass increase of the blade
- The CFRP straps also close the torsional box and thereby increases the induced twist

Characteristics	Design 2011	Design 2016
Lead Lag Bending Stiffness	7194 Nm <sup>2</sup>	26500 Nm <sup>2</sup>
Flap Bending Stiffness	174 Nm <sup>2</sup>	280 Nm <sup>2</sup>
Torsional Stiffness	169 Nm <sup>2</sup>	172 Nm <sup>2</sup>
Tensile Stiffness	$1.35 \cdot 10^7$ N	$2.95 \cdot 10^7$ N
Center of Gravity	25.9 % chord	25.5 % chord
Tension Center	19.2 % chord	25.5 % chord
Mass per Length	1.32 kg/m	1.47 kg/m
Twist	5.4 °	5.7 °

Figure 4: Comparison of calculated blade parameters at r/R=0.25

Beside the strain distribution further characteristics change, figure 4 shows a brief overview. The goal is to build a complete four-bladed rotor. To ensure that all blades have the same characteristics, each blade will have an identical structure, although they will be instrumented differently. In the less equipped rotor blades sensors will be replaced by dummies and sensor cables will remain. Since the first set of STAR blades show different properties between the blades, this approach is chosen to minimize any deviation. Furthermore, an identical blade design contributes to a more standardized manufacturing process, which also adds to the objective of similar blades. To get an impression of the highly detailed models which were generated, figure 5 shows the skin with integrated actuators (dark brown for GFRP, lighter brown for the actuators) and the inner design with spar and straps made of carbon fiber (grey). Furthermore the pressure sensors (light brown) next to the cable tree in green and in a very dark grey the balancing weights at the leading edge are shown.

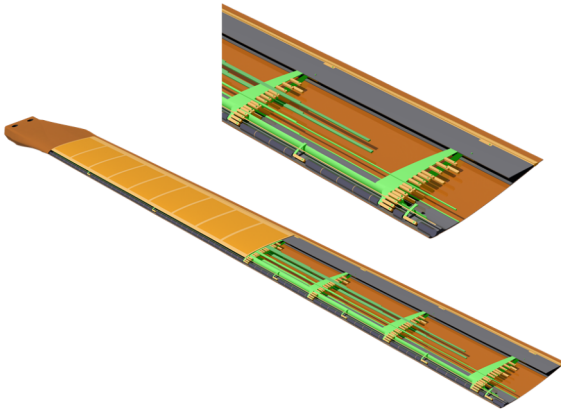


Figure 5: Detailed rotor blade Design, overall and detail

### 3 BLADE MANUFACTURING

In this paper, only a summary of the manufacturing details will be explained. The manufacturing process of highly instrumented rotor blades is very challenging. Due to the small size of the scaled blades, the manufacturing has to be very precise and allows only very little deviation in comparison to the digital design. The properties regarding stiffness and center of gravity have to meet the calculated ones. The rotor blade is manufactured in two mold halves and at the end of the process both halves are glued together. The general manufacturing concept includes a lot of individual steps, but can be roughly summarized as follows:

1. Manufacturing of the skins with integrated actuators, strain gauges and wiring
2. Manufacturing of additional carbon fiber straps
3. Milling the spar out of a CFRP-plate and milling out the foam core segments

4. Gluing of CFRP-straps, sensors and spar
5. Cable positioning, soldering and shielding
6. Adaption of foam to the inner skin structure (cables, straps)
7. Gluing of counter weights in the spar
8. Final assembly of mold halves using adhesive
9. Finishing works (electrical connectors, )

The manufacturing of the skin is one of the most challenging tasks within the blade manufacturing as the actuators, sensors and wires are directly integrated. There are 15 actuators and 25 strain gauges (9 for torsion, 9 for flap and 7 for lag) integrated into each skin half (see figure 6). The skin consists of 2 layers prepreg of GFRP material (Hex-ply913) and is cured in an autoclave. The use of prepreg provides high quality laminates with a predetermined and reproducible resin to fiber ratio.



Figure 6: Blade skin half with integrated actuators, strain gauges and wiring

As already mentioned, there are additional straps made of carbon fiber placed near to the trailing edge to reduce the loads at the actuators. The straps consist of 5 layers with a width of 25.6mm and a total thickness of 0.65mm. They are glued under vacuum with the two component epoxy ARALDITE 2011. The same carbon fiber material (M21E) is used for the spar. According to a layer plan numerous CFRP layers are stacked such that the root region has quasi-isotropic properties and the aerodynamic region has unidirectional properties. With this stack up a plate is manufactured. Afterwards, the complete spar contour is milled. Pressure sensor locations are omitted in the spar. The sensor cables are guided directly through the spar by a small opening (see figure 7). This is necessary because in contrast to previous designs, the core and belt of the spar are no longer manufactured separately from each other. The spar was made of glass fiber composite and the prepreg layers of the belt were cured in one step together with the skin layers. To minimize the risk through diverging thermal expansions for the sensitive and expensive rotor blade skin

such a procedure with a mixture of carbon and glass fiber has been rejected.

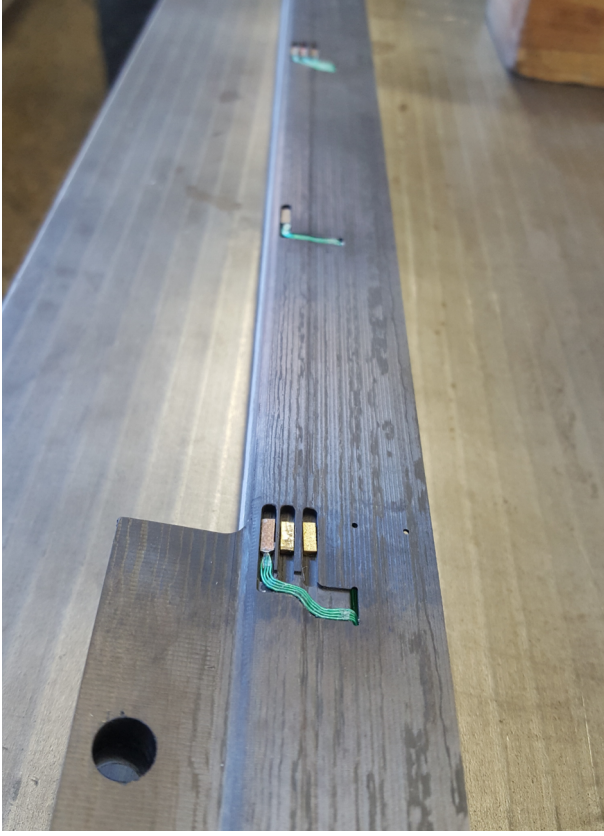


Figure 7: Carbon fiber spar with integrated pressure sensor dummies



Figure 8: Positioning of pressure sensors

At the lower left edge of figure 7 a kind of tongue at the spar can be seen. This tongue concept has been introduced to achieve improved positioning accuracy. Both, the skin and the spar are thus fixed and can no longer slip during the gluing or subsequent work within the mold. Various templates are used in order to position the pressure sensors within the skin. These are designed in CAD and finally 3d printed. They help to maintain the exact distances between the sensors, but also to place the cables (see figure 8). For the first prototype blade only dummies have

been used which are intended to represent the masses of the expensive pressure sensors. All dummy masses were provided with cables in order to obtain the same characteristics as the fully instrumented rotor blades manufactured later on. Furthermore, the manufacturing process can be practiced and improved.

Since not all rotor blades can be equipped with the maximum number of sensors. In less instrumented blades sensor dummies replace the pressure sensors. The number of cables remains the same, which is resulting in a huge number of sensor cables. In the highest instrumented rotor blade, nearly 100 pressure sensors are to be installed. Each pressure sensor includes 4 cables. This means that, along with the cables of the strain gauges and the actuators, over 550 cables with a total length of more than 600 m have to be integrated in a very limited assembly space. This is an enormous challenge.



Figure 9: Manufacturing of ribbon cables

Due to the large amount of cables which have to be integrated in all rotor blades, the individual cables are pre-assembled, combined and manufactured as ribbon cables (see figure 9). These ribbon cables can be precisely positioned with a still high but significantly reduced effort. After that they are glued with a thin adhesive film.



Figure 10: Finished cabling and shielding

Figure 10 shows the finished placement of all cables. The cables of the pressure sensors (green), strain gauges (multicolored) and the actuators (red) were separated from each other. Experiences from previous projects (see<sup>[6]</sup>) have shown that the high voltage cables of the actuators

influence the sensor signals. For this reason, all cables are inserted into a copper mesh in order to minimize electromagnetic interferences. The position of the individual cable assemblies is a compromise between the EMI problem and the mechanical properties, e.g. the position of the center of gravity. Furthermore, in figure 10 the carbon fiber reinforcement near the trailing edge is easily visible. Worthwhile to notice are the connection points of the actuators. These must be absolutely insulated from the electrically conductive carbon fiber reinforcement.

The foam parts, which have already been milled in shape, must be brought into their final contour. This means, the reinforced carbon straps, routing of the cables or other unevenness must be removed from the foam before they are finally glued into the mold halves. After milling to the parting plane, the balancing weights can be inserted into the leading edge and glued with epoxy. Finally, both mold halves are glued together. After demolding, the final works on the outer contour are following, for example, drilling the bolt holes into the root or integrating LEDs into the blade tip.



Figure 11: Wiring at the blade root

The last challenge is the cabling in the connector housing. All sensors and actuators must be soldered to a variety of plugs. For the sensors, a special circuit board is used. A specially designed amplifier card sends the amplified signals from the rotor blade to the non-rotating system. Figure 11 gives an overview of the complexity and effort behind this step.

The manufacturing of the first rotor blade prototype based on the new design was finished in the middle of 2017 and subsequently tested in the laboratory.

## 4 EXPERIMENTAL EVALUATION OF STRUCTURAL BLADE PROPERTIES

The newly designed rotor blade is experimentally tested regarding structural properties and results are compared to the previously tested STAR rotor blades<sup>[7:8]</sup>. The test set-ups are nearly identical between old and new measurements. The following properties regarding the airfoil region are measured and compared:

- Torsional stiffness
- Flap bending stiffness
- Chordwise position of the elastic axis
- Active twist angle with actuators

### 4.1 Measurement of torsional and flap bending stiffness as well as elastic axis

Torsional and flap bending stiffness as well as the elastic axis are determined in the laboratory for the airfoil region between its initial radial position and the end of the actuator area. Segments with modifications of the cross section due to implemented pressure sensors and contacts are considered to be of small radial extension compared to the blade length. Consequently, the structural properties are determined based on the assumption that the blades possess a uniform cross section design over the regarded region. Accordingly, the obtained structural properties represent averaged values.

#### 4.1.1 Test setup

The first three properties were determined in one test setup. The blade is clamped at the bolts and hold in an upward position as shown in the left picture of figure 12.



Figure 12: left: Test rig with rotor blade; right: Rotor blade clamp

Additionally, it was fixed at the beginning of the airfoil region using an airfoil shaped clamp (figure 12, right). The blade was then loaded like a single side supported beam by an external force at the end of the actuator area within the airfoil region. Therefore, another clamp was mounted at the end of the actuator area near to the blade tip. The clamp

was extended in chordwise direction such that it could be used as a lever for force application. The leading edge of the profile was defined as zero on the lever.

The force was applied perpendicular to the radial blade axis and the clamp at the end of the actuator by a string. The string was pulled by an excenter rotating with 0.3 Hz to avoid creeping effects of the glass fiber composite material of the rotor blade. At the other end the string was attached to a load cell, to relate the displacements to their corresponding forces. The point of application of the force can be changed along the lever.

The blade deformation was measured with a photogrammetric system for the STAR blades and with a laser profile scanner for the prototype blade. Both systems can determine the in plane movement of the clamp perpendicular to the spanwise direction. A schematic of the test setup is shown in figure 13

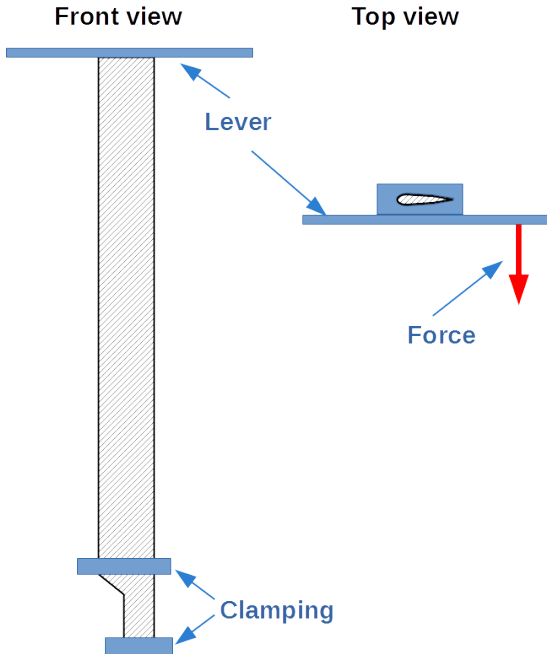


Figure 13: Test setup schematic

#### 4.1.2 Calculating stiffness and elastic axis from in plane deformation and force

In order to calculate the desired properties from the in plane movements of the clamp it was taken into account that any force  $F$  applied to the cross section is equivalent to the same force applied to the elastic axis combined with a moment  $F \cdot d$  as shown in figure 14.

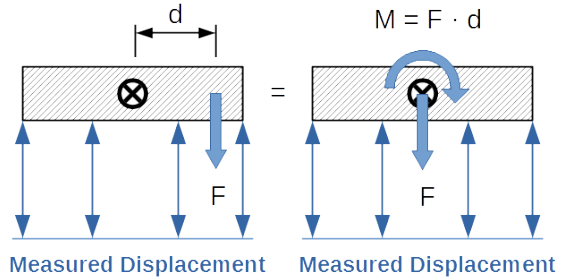


Figure 14: Measuring and Calculation schematic

Accordingly resulting displacements  $w$  in profile thickness direction with varying force application points along the clamp and lever were measured.

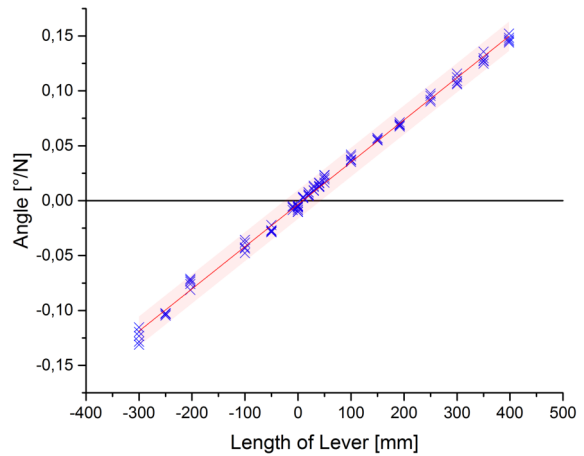


Figure 15: Lever Displacements

The position of the elastic axis and thus length  $d$  is unknown. Therefore the data was used to calculate an angle of rotation. By interpolation the position with no rotational angle and thus a zero moment  $M_T$  could be determined, shown in figure 15.

As a zero moment  $M_T$  can only be obtained when  $d$  is zero. The elastic axis of the rotor blade is the point in figure 15 where the linear regression of angle and length of lever cross the  $0^\circ/N$ -axis. Knowing the position of the elastic axis, the applied moment  $M_T$  was derived for every single measurement and then related to the rotational angle  $\vartheta_l$  and the length  $l$  between the clampings, resulting in the torsional stiffness  $GI_T$  of the rotorblade:

$$GI_T = \frac{M_T l}{\vartheta_l}$$

Likewise the displacement  $w$  was derived at the position of the elastic axis for every single measurement and correlated to the force  $F$  and the length  $l$  between the clamps, resulting in the flap bending stiffness  $EI_{flap}$ :

$$EI_{flap} = \frac{l^3 \cdot F}{3 \cdot w}$$

#### 4.1.3 Results and Discussion

Using the test set-up described in the previous section, the position of the elastic axis can be determined. For the prototype blade the linear regression is shown in figure 15 resulting in a position of 10,54 mm from the leading edge which translates to 8,7% chord length. A comparison of the elastic axis of STAR rotor blades with the prototype blade is given in figure 16.

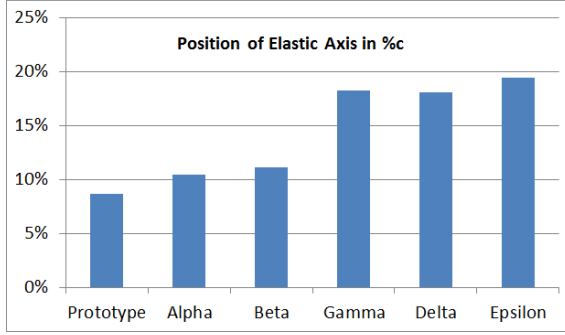


Figure 16: Comparison of elastic axis positioning between new and old design

The chordwise position of the elastic axis matches roughly that of the alpha and beta blade and lays far in front of the gamma, delta and epsilon blade. The prototype blade, alpha and beta have in common, that they all have integrated cables for a high grade of instrumentation. Most of these cables are positioned at the c-shape of the spar. With this positioning near to the leading edge the elastic axis moves in this direction, too. For the prototype blade the even higher cable amount and the stiffness cause the elastic axis to move forward even more.

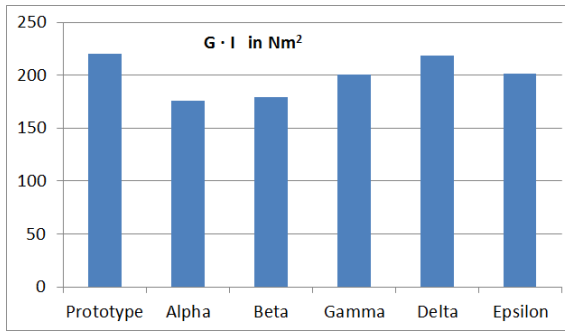


Figure 17: Comparison of torsional stiffness between new and old design

Figure 17 shows a higher overall torsional stiffness in comparison to the alpha and beta blade. The other three blades will not be considered in this case, because of their low instrumentation grade. The higher stiffness of the prototype blade is caused by the stiffer spar and the additional carbon fiber straps at the trailing edge. The flap bending stiffness of the prototype blade, is about 1.7 times greater than the stiffest of the STAR blades. This is due to the fact

that carbon fiber is integrated into the truss and the trailing-edge strap to increase lag bending and tensile stiffness, which also increases flap bending stiffness.

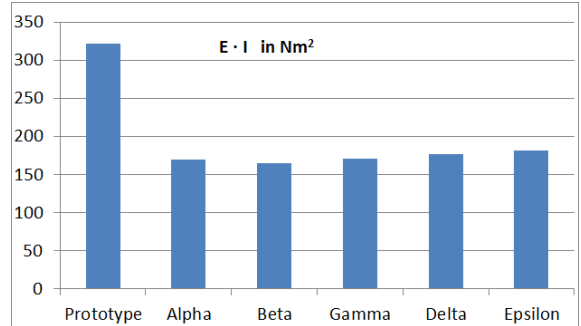


Figure 18: Comparison of flap bending stiffness between new and old design

#### 4.2 Measurement of Active Twist Angle

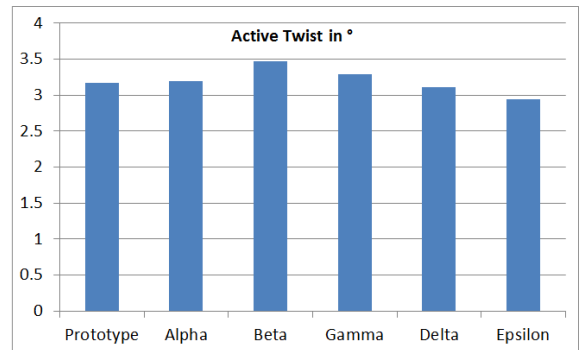


Figure 19: Comparison of active twist between new and old design

Lastly the active twist angle is measured. The same setup as for the stiffness measurements is used with the exception that the rotor blade is solely clamped at the bolts. Again the angle for the STAR blades was measured with a photogrammetry system, while the prototype blade was measured with a laser profile scanner. As can be seen in figure 19 the active twist is near the mean of the values of the STAR blades.

##### 4.2.1 Results and Discussion

Despite the fact, that the overall torsion stiffness is higher than for the alpha and beta blade the active twist remains at a similar value. Most of the actuator region does not suffer a higher local stiffness and thus the influence on the actuator elongation is small. Because of the additional closing of the torsional box at the trailing edge by the carbon straps, the actuator movement is transformed into a twist movement more efficiently.

#### 4.3 First whirltower tests

After laboratory investigations a very first test in the whirltower was conducted. A detailed analysis of the data is still

pending, but initial results show a general reduction of the strains, close to the simulated results. In the experiment strain distributions are measured at several radial positions and different rotor speeds. Furthermore, it can be clearly seen that the design changes have an effect on the strain distribution. As expected the position of the tension axis is close to the center of gravity. In comparison to the previous design the axis is even behind the center of gravity. This results in a small pivoting deflection to the trailing edge, which leads to a compressive preload of the actuators at the trailing edge region. This has a positive effect on the durability of the actuators.



Figure 20: Investigations of the efficiency of the prototype blade design in centrifugal test rig

## 5 CONCLUSION AND OUTLOOK

The actuators embedded in an active twist rotor blade are subject to considerable loads due to the high centrifugal force. Based on the DLR project STAR<sup>[6]</sup>, an active rotor design has been completely revised. The new design includes several material and structural adjustments. A revised actuator design is applied. The loads in the actuator system were significantly reduced to a noncritical amount and furthermore distributed evenly by using carbon fiber composite for the spar and placed additional straps near to the trailing edge. Hereby, most likely the fatigue problems of the actuators will be overcome. Furthermore manufacturing as-

pects have been presented within this paper. An important objective is the similarity of the individual rotor blades and its properties. To achieve this and due to the high requirements as well as the limited assembly space a detailed manufacturing concept is vital. Even though high effort was put into this, many challenges throughout the manufacturing process arose and had to be solved. The manufacturing of a rotor blade prototype was finished in the middle of 2017 and proved to be very useful as a basis for manufacturing the complete rotor blade set. The experimental results validate the simulations in most aspects and are as such very promising. Further tests of the prototype rotor blade regarding its active twist behavior and durability of the actuators have to be completed. After finishing this qualification phase, the manufacturing of a complete rotor blade set represent the next step on the way to the planned wind tunnel test in the German-Dutch wind tunnel (DNW).

## Glossary

$EI_{flap}$  flap bending stiffness

$F$  force

$GI_T$  torsional stiffness

$M_T$  torsional moment

$\vartheta_l$  rotational angle

$d$  length of lever

$l$  length between clamps

$w$  displacement in direction of the profile thickness

## References

- [1] A. Büter and E. Breitbach. Adaptive blade twist - calculations and experimental results. In Associazione Italiana di Aeronautica ed Astronautica, editor, *25. European Rotorcraft Forum, Rom, Italy, Sep. 1999*, volume VOL 2, 1999.
- [2] Christoph K. Maucher, Boris A. Grohmann, and Peter Junker. Review of adaptive helicopter rotor blade actuation concepts. In *Adaptronic Congress*, 2006.
- [3] Hans Peter Monner, Steffen Opitz, Johannes Riemenschneider, and Peter Wierach. Evolution of active twist rotor designs at dlr. In *49th AIAA/ASME/ASCE/AHS/ASC Structures, Structural Dynamics, and Materials Conference*, April 2008.
- [4] Hans Peter Monner, Johannes Riemenschneider, Steffen Opitz, and Martin Schulz. Development of active twist rotors at the german aerospace center (dlr). In *16th AIAA/ASME/AHS Adaptive Structures Conference*, April 2011.
- [5] Peter Wierach, Johannes Riemenschneider, Steffen Opitz, and Frauke Hoffmann. Experimental investigation of an active twist model rotor blade under centrifugal loads. In *EFR 2007*, September 2007.

- [6] Steffen Kalow, Steffen Opitz, Johannes Riemenschneider, and Frauke Hoffmann. Results of a parametric design study to adapt the structural properties and strain distribution of active twist blades. In *AHS 2016*, Mai 2016.
- [7] Johannes Riemenschneider, Ralf Keimer, and Steffen Kalow. Experimental bench testing of an active-twist rotor. In *ERF (European Rotorcraft Forum)*, September 2013.
- [8] Frauke Hoffmann, Oliver Schneider, Berend G. van der Wall, Ralf Keimer, Steffen Kalow, Andre Bauknecht, Benjamin Ewers, Kurt Pengel, and Gerrit Feenstra. Star hovering test - proof of functionality and representative results -. In *40th European Rotorcraft Forum*, number 10-B in Conference Proceedings online, pages 1–19, September 2014.